

SAC-LoCo: Safe and Adjustable Compliant Quadrupedal Locomotion

Aoqian Zhang¹, Zixuan Zhuang², Chunzheng Wang¹, Shuzhi Sam Ge¹, Fan Shi¹ and Cheng Xiang¹

Abstract—Quadruped robots are designed to achieve agile and robust locomotion by drawing inspiration from legged animals. However, most existing control methods for quadruped robots lack a key capacity observed in animals: the ability to exhibit diverse compliance behaviors while ensuring stability when experiencing external forces. In particular, achieving adjustable compliance while maintaining robust safety under force disturbances remains a significant challenge. In this work, we propose a safety-aware compliant locomotion framework that integrates adjustable disturbance compliance with robust failure prevention. We first train a force-compliant policy with adjustable compliance levels using a teacher–student reinforcement learning framework, allowing deployment without explicit force sensing. To handle disturbances beyond the limits of compliant control, we develop a safety-oriented policy for rapid recovery and stabilization. Finally, we introduce a learned safety critic that monitors the robot’s safety in real time and coordinates between compliant locomotion and recovery behaviors. Together, this framework enables quadruped robots to achieve smooth force compliance and robust safety under a wide range of external force disturbances.

I. INTRODUCTION

Compliance is a fundamental principle of locomotion observed in both humans and animals. When subjected to external forces, legged animals exhibit versatile responses: they may resist or yield to the disturbance. More importantly, under strong perturbations, animals instinctively move in the direction of the applied force to preserve balance and prevent falls. Achieving such safe and compliant behaviors in legged robots is essential for reliable real-world operations under external forces. Beyond self-protection, adjustable compliance could potentially broaden the range of future applications, such as enhancing adaptability in complex environments, enabling safer human-robot interaction, and supporting cooperative tasks.

Reinforcement learning (RL) controllers have been shown to be highly effective in allowing quadruped robots to perform a wide range of tasks, such as complex terrain traversal [1], physical interaction with objects [2], [3], and obstacle avoidance [4]. Although RL-based controllers enable diverse whole-body behaviors, achieving robust and adaptive response to external forces remains a significant challenge. Most existing approaches emphasize strict task execution, such as tracking velocity or position regulation [5], [6], while neglecting the effects of large or persistent external disturbances. Although deep RL inherently provides some robustness to perturbations, achieving versatile responses

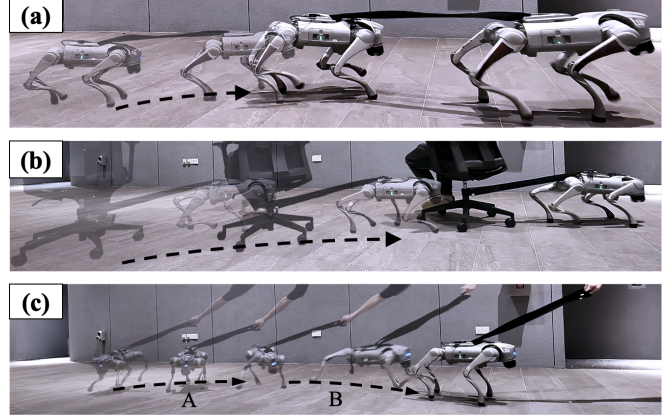


Fig. 1. (a) Quadruped robot compliantly follow the leader robot. (b) Quadruped robot pulling a human on a chair. (c) A: Quadruped robot move along with a pulling force compliantly and B: jump toward the pulling force to restore balance.

across a broader range of external forces requires more sophisticated learning strategies. To this end, both model-based approaches [7] and learning-based methods [8] have been explored for disturbance adaptation. However, these methods often produce limited behavioral diversity, leading to failures when facing large or prolonged disturbances. This highlights the need for a locomotion controller that can diversify its response to external disturbances through adjustable compliance, enabling it to resist or yield with applied forces while maintaining robust stability.

To address this challenge, we propose SAC-LoCo, a safe and adjustable compliant quadrupedal controller that integrates a velocity-based force compliant controller with a safety-oriented recovery controller. A learned safety critic is proposed to detect and prevent potential failures promptly. The main contributions of this work are as follows:

- An external force compliant locomotion policy trained with a teacher-student reinforcement learning framework, enabling a wide range of adjustable compliance behavior without requiring explicit force sensing.
- A safe policy grounded in the capture-point dynamics for robot recovery from dangerous states and stabilization under large force disturbance.
- A learned safety critic that evaluates the robot’s recoverability, ensuring smooth compliance under safe interactions and timely recovery when destabilized by large disturbances.
- Extensive simulations and hardware experiments validate the effectiveness of the proposed method.

¹Department of Electrical and Computer Engineering, National University of Singapore, Singapore

²School of Computer Science and Engineering, Sun Yat-sen University, China

II. RELATED WORKS

For external force-compliant and safe control of legged robots, some existing work adopts model-based methods to estimate the external forces acting on the robot. Khandelwal et al. proposed a method using only proprioceptive feedback to estimate the external forces [9], which has been shown to provide force estimations that can be directly leveraged by an admittance controller for payload transportation. Beyond using proprioceptive information, Kang et al. proposed multimodal sensing by combining IMU and vision data to estimate external forces and moments through factor graph optimization [7]. The estimated forces can then be incorporated into a model predictive control (MPC) framework to optimize footstep placement for disturbance rejection. Despite these advances, existing model-based approaches have two key limitations: (i) they are typically restricted to handling small perturbations (less than 50N), and (ii) they rely on pre-defined gaits, which constrain the robot to low-speed locomotion. These limitations significantly undermine the robot’s ability to respond effectively to large, impulsive external forces.

Reinforcement learning (RL) based methods, on the other hand, demonstrate stronger generalization and robustness to larger impulse disturbances. For example, Hartmann et al. proposed a multi-stage episodic training setup with reward shaping for robots to respond less aggressively to transient perturbations [10]. However, this approach is still not effective against large persistent forces. Inspired by biomechanics, Li et al. proposed a torque-based policy that directly outputs joint-level torques such that the quadruped robot can adapt to sudden disturbances acting on the legs and exhibits compliance to external forces in all directions [11]. However, the resulting fixed compliance prevents the robot from reliably following velocity commands under external pushes and doesn’t incorporate adjustable compliance behavior. To address this limitation, Zhou et al. proposed to apply hierarchical reinforcement learning for active compliance control [12]. In this framework, a high-level RL planner modulates velocity commands according to estimated external forces so that the robot can actively follow velocity targets while complying with external forces. Despite its advantages, the method has notable limitations: (i) the force estimation module is trained jointly with the low-level policy, which removes the necessity of the high-level RL planner, and (ii) modifying compliance parameters requires retraining the high-level policy, limiting flexibility and efficiency. Concurrently with our work, Xu et al. proposed a RL framework that integrates a virtual mass-spring-damper model for reference generation and tracking [13]. This approach enables robust velocity compliance with adjustable compliance levels. However, its success rate decreases when external forces exceed 500N, highlighting the limitation of relying on a single policy to achieve both precise velocity tracking and high force tolerance. Our work, in comparison with existing methods, has several advantages as shown in Table I.

TABLE I

COMPARISON OF DIFFERENT METHODS (M: MODEL-BASED, L: LEARNING-BASED). ES: NO EXTRA SENSOR REQUIRED, VC: VELOCITY COMPLIANCE, AC: ADJUSTABLE COMPLIANCE LEVEL IN A UNIFIED POLICY, LT: LARGE IMPULSE TOLERATION.

Method (paradigm)	ES	VC	AC	LT
Kang et al. [7] (M)	✗	✗	✗	✗
Hartmann et al. [10] (L)	✓	✗	✗	✗
Zhou et al. [12] (L)	✓	✓	✗	✗
Xu et al. [13] (L)	✓	✓	✓	✗
SAC-LoCo (L)	✓	✓	✓	✓

III. METHODS

We present SAC-LoCo, a safety-aware locomotion control framework composed of three learned modules as illustrated in Fig. 2: (i) a compliant policy with adjustable compliance level under external disturbances (Section III-B), (ii) a safe policy designed to recover the robot from unsafe states and stabilize it under large disturbances (Section III-C), and (iii) a safety critic that evaluates the safety of the current state and activates the safe policy when recovery is required (Section III-D).

A. Problem Formulation

We consider quadrupedal locomotion under external disturbances, where the robot receives a command $\mathbf{c} = [v'_x, v'_y, \omega'_z, k]$ specifying a command linear velocity in robot’s body frame, a command angular velocity about the z -axis and a tunable compliance level parameter. In the presence of an external force disturbance in robot’s body frame $\mathbf{F} = [F_x, F_y, F_z]$, the control objective is to track the command velocity while exhibiting adjustable compliance to the external disturbances, yielding more to the force for larger values of k and resisting more for smaller values of k . When the external disturbance becomes sufficiently large and may drive the robot into unsafe states, the control objective shifts to restore balance and stabilize the robot. In this work, a failure is defined as the quadruped robot’s base making contact with the ground or the robot falling over. At each control step t , the control policies are executed on the quadruped robot using only proprioceptive sensing and generate joint-level actions. The observable states of the robot is given by

$$\mathbf{s}_t = [\mathbf{g}_t, \boldsymbol{\omega}_t, \mathbf{q}_t, \dot{\mathbf{q}}_t, \mathbf{a}_{t-1}, \mathbf{c}_t], \quad (1)$$

where $\mathbf{g}_t \in \mathbb{R}^3$ denotes projected gravity, $\boldsymbol{\omega}_t \in \mathbb{R}^3$ the body angular velocity, $\mathbf{q}_t, \dot{\mathbf{q}}_t \in \mathbf{R}^{12}$ the joint positions and velocities, $\mathbf{a}_{t-1} \in \mathbb{R}^{12}$ the previous actions, and $\mathbf{c}_t \in \mathbb{R}^4$ the command. The actions $\mathbf{a}_t \in \mathbb{R}^{12}$ of the control policies are the target joint positions \mathbf{q}_t^* , tracked by a low-level proportional-derivative (PD) controller that computes joint torques $\boldsymbol{\tau}_t = K_p (\mathbf{q}_t^* - \mathbf{q}_t) + K_d (-\dot{\mathbf{q}}_t)$, where K_p and K_d denote the proportional and derivative gains, respectively.

B. Compliant Policy Training

To achieve compliance behavior, a velocity modulator calculates the desired velocity $\mathbf{v}^* = [v_x^*, v_y^*]$ based on the

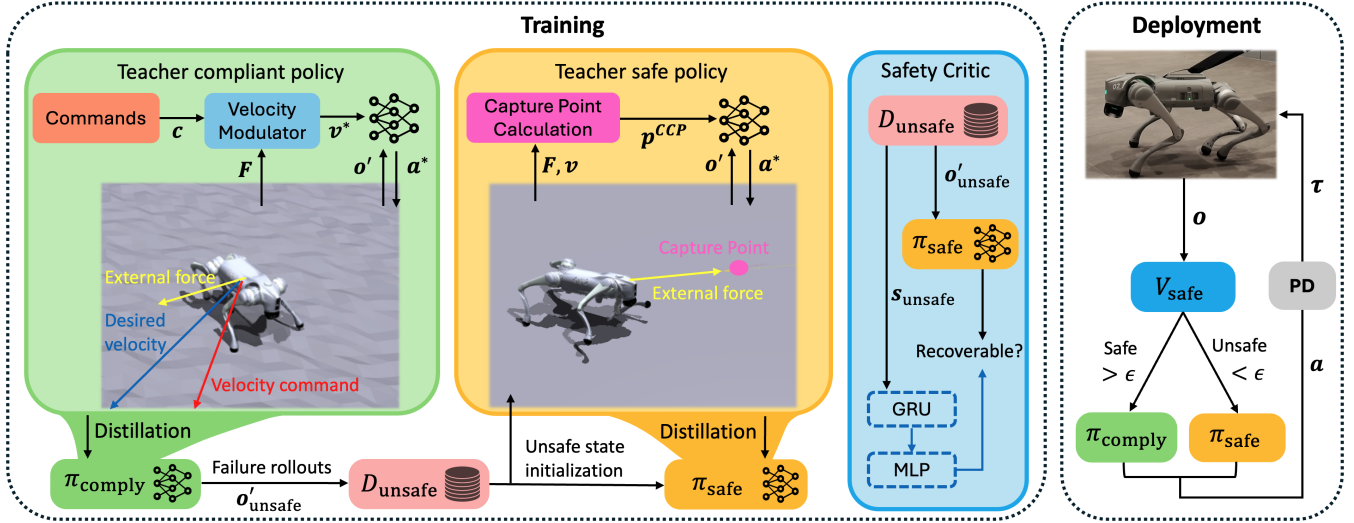


Fig. 2. Overview of SAC-Loco. The teacher compliant policy π_{comply}^* with velocity modulation is first trained using privileged observations. It is then distilled into a student compliance policy π_{comply} . The failure rollouts from π_{comply} are collected into an unsafe dataset $\mathcal{D}_{\text{unsafe}}$. A teacher safe policy π_{safe}^* is trained to recover from unsafe states initialized from $\mathcal{D}_{\text{unsafe}}$ and other large force disturbances using capture point dynamics. After distilling into the student safe policy π_{safe} , a safety critic V_{safe} is trained to estimate the recoverability of π_{safe} . During deployment, V_{safe} selects the policy to control the robot.

external force

$$v_x^* = \text{clip}(v'_x + kF_x, -v_{x,\max}, v_{x,\max}), \quad (2)$$

$$v_y^* = \text{clip}(v'_y + kF_y, -v_{y,\max}, v_{y,\max}). \quad (3)$$

The desired velocity, if followed by the robot, would enable the robot to achieve adjustable compliance behaviors under external force disturbances. To train a policy that tracks the desired velocity without external force information, we first train a teacher force compliant policy π_{comply}^* using additional privileged observations obtained in simulations

$$\mathbf{o}'_t = [z_t, \mathbf{Q}_t, \mathbf{v}_t, \mathbf{F}_t, \boldsymbol{\tau}_{\text{ext},t}], \quad (4)$$

where $z_t, \mathbf{Q}_t \in \mathbb{R}^4$, $\mathbf{v}_t \in \mathbb{R}^3$, $\mathbf{F}_t \in \mathbb{R}^3$, and $\boldsymbol{\tau}_{\text{ext},t} \in \mathbb{R}^3$ correspond to base height, body orientation in quaternions, body velocity, external force and external torque disturbances, respectively. We design the velocity tracking rewards to enable the robot to follow the desired velocity \mathbf{v}^* computed by the velocity modulator. Regularization rewards are included to help robot maintain stable posture and smooth joint level actions. The detailed reward terms and corresponding weights are shown in Table II.

After training π_{comply}^* , we distill it into student policies π_{comply} that can be deployed on the physical robot using only the observable states defined in (1). To compensate for the lack of privileged information, the student's policy receives as input a stacked observation history of length 20

$$\mathbf{o}_t = [s_{t-20}, s_{t-19}, \dots, s_{t-1}, s_t]. \quad (5)$$

To achieve efficient training and a balance between exploration and exploitation, we use the PPO distillation method in [14]. We compute the mean squared error loss between the teacher's actions and the student's actions

$$\mathcal{L}_{\text{distillation}} = \|\pi^*(\mathbf{o}'_t) - \pi(\mathbf{o}_t)\|_2^2, \quad (6)$$

and the total loss for PPO becomes

$$\mathcal{L}_{\text{total}} = \alpha \mathcal{L}_{\text{distillation}} + \beta \mathcal{L}_{\text{PPO}}. \quad (7)$$

To facilitate early stage exploration in the correct direction, we also added two additional reward terms inspired by [15] to guide the student policy's actions to stay close to the teacher policy's actions

$$r_{\text{action}} = \exp\left(-\frac{\|\mathbf{a}_t^* - \mathbf{a}_t\|^2}{0.5}\right), \quad r_{\text{direction}} = \exp\left(\frac{\mathbf{a}_t \cdot \mathbf{a}_t^*}{\|\mathbf{a}_t\| \|\mathbf{a}_t^*\|}\right), \quad (8)$$

where \mathbf{a}_t^* and \mathbf{a}_t are the teacher's and student's actions, respectively. To increase training efficiency, we adopt asymmetric PPO, where the critic additionally observes the privileged observation \mathbf{o}'_t in (4).

C. Safe Policy Training

The safe policy's objective is to prevent failure under large force disturbances by actively restoring balance of the robot. Based on the linear inverted pendulum model [16], the Corrected Capture Point (CCP) determines the required planar displacement of the support polygon centroid (SPC) of the quadruped robot to neutralize external forces [7]. We calculated the position of SPC for a quadruped robot as

$$\mathbf{p}_t^{\text{cent}} = \begin{cases} \frac{1}{|\mathcal{S}_t|} \sum_{i \in \mathcal{S}_t} \mathbf{p}_{i,t}, & \text{if } |\mathcal{S}_t| \geq 2, \\ \mathbf{p}_t^{\text{base}}, & \text{if } |\mathcal{S}_t| < 2, \end{cases} \quad (9)$$

where $\mathcal{S}_t \in \mathbb{R}^2$ is the set of supporting feet at time t , $\mathbf{p}_{i,t} \in \mathbb{R}^2$ is the planar position of foot i and $\mathbf{p}_t^{\text{base}} \in \mathbb{R}^2$ is the planar position of robot's base. To restore balance under external forces, $\mathbf{p}_t^{\text{cent}}$ needs to be shifted to $\mathbf{p}_t^{\text{CCP}} =$

$\mathbf{p}_t^{\text{cent}} + [\delta x_t, \delta y_t]^\top$ by the planar offsets

$$\delta x_t = \sqrt{\frac{z_t}{g}} v_{x,t} + \frac{F_{x,t} z_t}{mg}, \quad (10)$$

$$\delta y_t = \sqrt{\frac{z_t}{g}} v_{y,t} + \frac{F_{y,t} z_t}{mg}, \quad (11)$$

where z_t is the base height of the robot, m is the mass of the robot and g is the gravitational constant. For a quadruped robot, due to its structural anisotropy, it can sustain a larger force in the longitudinal (x -axis) direction than in the lateral (y -axis) direction. Therefore, we further compute a yaw orientation offset

$$\delta\psi = \begin{cases} \text{atan2}(F_y, F_x), & \text{if } F_x \geq 0 \\ \text{atan2}(F_y, F_x) + \pi, & \text{if } F_x < 0 \end{cases}, \quad (12)$$

to align the robot's x -axis with the disturbance force. When the force acts toward the robot's front, the robot aligns its heading with the force direction; when the force acts toward the rear, the robot aligns its tail with the force direction, thereby converting lateral disturbances into longitudinal ones.

In order for the robot to adjust its $\mathbf{p}_t^{\text{cent}}$ to $\mathbf{p}_t^{\text{CCP}}$ as fast as possible, we train a teacher safe policy π_{safe}^* in two stages. In Stage I (Pose tracking), we randomly sample target offset $\delta x, \delta y \sim \mathcal{U}(-3\text{m}, 3\text{m})$ and $\delta\psi \sim \mathcal{U}(-\pi\text{rad}, \pi\text{rad})$, training the robot to track any pose as fast as possible. In Stage II (Disturbance recovery), we start exerting external forces on the robot and calculate $\delta x_t, \delta y_t$ and $\delta\psi_t$ at each timestep using (10) - (12). This policy takes the same observation as (4), with \mathbf{c}_t replaced by $\delta x_t, \delta y_t$ and $\delta\psi_t$. We design reward functions to minimize the position tracking error $p_t^{\text{err}} = \|\mathbf{p}_t^{\text{cent}} - \mathbf{p}_t^{\text{CCP}}\|_2$ between the robot's SPC and target CCP, and the yaw orientation offset $\delta\psi$. The detailed reward terms and their corresponding weight are shown in Table II. After training π_{safe}^* , we distill it into the student safe policy π_{safe} using the same distillation method in Section III-B.

D. Safety Critic Training

To enable timely switching from the compliant policy π_{comply} to the safe policy π_{safe} before failure occurs, we train a safety critic V_{safe} that evaluates the robot's observations in real time. Unlike prior policy switching approaches (e.g. [4], [17]), which rely on fixed policy switching rules or only condition on a single policy, our proposed critic leverages information from both policies during training and serves as a policy switching mechanism with more robustness guarantee. We first collect rollouts of π_{comply} in simulation under random commands and external disturbances. When a failure occurs, the 150 preceding timesteps' privileged observations $\mathbf{o}'_{\text{unsafe}}$ in (4) which contain the observable states $\mathbf{s}_{\text{unsafe}}$ in (1) are stored to an unsafe dataset $\mathcal{D}_{\text{unsafe}}$. The dataset $\mathcal{D}_{\text{unsafe}}$ serves two purposes. First, during Stage II training of π_{safe} , $\mathbf{o}'_{\text{unsafe}} \sim \mathcal{D}_{\text{unsafe}}$ are used as state initialization, helping π_{safe} to practice recovery from potentially dangerous conditions. Second, after π_{safe} is trained, we initialize environment with $\mathbf{o}'_{\text{unsafe}} \sim \mathcal{D}_{\text{unsafe}}$ and execute π_{safe} to determine whether it can recover the robot or not. The success and failure labels

TABLE II

PRIMARY REWARD FUNCTIONS FOR π_{COMPLY} (MARKED †), π_{SAFE} (MARKED *), SHARED REGULARIZATION TERMS (NO MARK), AND THEIR CORRESPONDING WEIGHTS.

Name	Expression	Weight
Linear velocity tracking †	$\exp\left(-\frac{\ v_{xy}^* - v_{xy}\ _2}{0.25}\right)$	1.0
Angular velocity tracking †	$\exp\left(-\frac{(\omega_z^* - \omega_z)^2}{0.25}\right)$	0.5
Position tracking soft *	$\frac{1}{1+p^{\text{err}2}}$	20.0
Position tracking tight *	$\frac{1}{1+(p^{\text{err}}/0.25)^2}$	20.0
Yaw angle tracking *	$\frac{1}{1+(\delta\psi/0.5)^2}$	20.0
Velocity direction *	$\max\left(0, \frac{v_x \delta x + v_y \delta y}{p^{\text{err}}}\right)$	40.0
Yaw rate direction *	$\dot{\psi} \cdot \text{sign}(\delta\psi)$	20.0
Stand still *	$(\ v_{xy}\ < 0.5 \wedge \dot{\psi} < 0.1) \cdot \mathbf{1}_{\text{reached}}$	20.0
Base height	$(z - 0.25)^2$	-0.5
Angular velocity penalty	$\ \omega_{xy}\ ^2$	-0.05
Joint torques	$\ \tau\ _2^2$	-0.0005
Joint velocities	$\ \dot{q}\ _2^2$	-0.0001
Joint accelerations	$\left\ \frac{\dot{q}_{t-1} - \dot{q}_t}{dt}\right\ ^2$	-2.5e-7
Action rate	$\left\ \frac{\dot{a}_{t-1} - \dot{a}_t}{dt}\right\ ^2$	-0.01
Joint angle limit	$\sum_{i=1}^{12} (q_i - 0.9 \cdot q_{i,\text{lim}})$	-10.0
Joint velocity limit	$\sum_{i=1}^{12} (\dot{q}_i - 0.9 \cdot \dot{q}_{i,\text{lim}})$	-5.0
Joint torque limit	$\sum_{i=1}^{12} (\tau_i - 0.85 \cdot \tau_{i,\text{lim}})$	-5.0
Collision	$F_{\text{base, thigh, calf}} > 0$	-10.0

associate with each $\mathbf{o}'_{\text{unsafe}}$ are added to $\mathcal{D}_{\text{unsafe}}$. Finally, V_{safe} is trained on $\mathbf{s}_{\text{unsafe}}$ and labels from $\mathcal{D}_{\text{unsafe}}$ via supervised learning using gradient descent. The data collection and training process for V_{safe} is shown in Algorithm 1. During deployment, the output of $V_{\text{safe}}(\mathbf{s}_t) \in [0 \sim 1]$ will be compared to a safety threshold ϵ . If output of V_{safe} falls below ϵ , π_{safe} will be activated to control the robot.

Algorithm 1 Safety Critic Training

- 1: Init $\mathcal{D}_{\text{unsafe}} \leftarrow \emptyset$ and V_{safe}^θ
- 2: **while** executing of π_{comply} under disturbances **do**
- 3: **if** failure occurs at time t **then**
- 4: $\mathcal{D}_{\text{unsafe}} \leftarrow \mathcal{D}_{\text{unsafe}} \cup \{\mathbf{o}'_{t-k}\}_{k=0}^{150}$
- 5: **end if**
- 6: **end while**
- 7: Train π_{safe} with $\mathbf{o}'_{\text{unsafe}} \sim \mathcal{D}_{\text{unsafe}}$ as state initialization
- 8: **for each** $\mathbf{o}'_{\text{unsafe}} \sim \mathcal{D}_{\text{unsafe}}$ **do**
- 9: Initialize environment with $\mathbf{o}'_{\text{unsafe}}$ and execute π_{safe}
- 10: $y \leftarrow \mathbb{I}[\text{successful recovery}]$
- 11: Assign label y to $\mathbf{o}'_{\text{unsafe}}$ in $\mathcal{D}_{\text{unsafe}}$
- 12: **end for**
- 13: **for each** optimization step **do**
- 14: Sample batch $(\mathbf{s}_{\text{unsafe}}, y) \sim \mathcal{D}_{\text{unsafe}}$
- 15: $\mathcal{L} \leftarrow \text{BCELoss}(V_{\text{safe}}(\mathbf{s}_{\text{unsafe}}; \theta), y)$
- 16: $\theta \leftarrow \theta - \eta \nabla_\theta \mathcal{L}$
- 17: **end for**

E. Training details

We train all policies in the Isaac Gym simulator [18] using 4096 environments in parallel. We use PPO algorithm [19] for policy optimization. The policy networks are parameterized as multi-layer perceptrons (MLPs) with hidden

layer sizes [512,256,128]. The safety critic consists of a two-layer GRU with hidden size 256, followed by an MLP head with layers [128,64]. We employ curriculum learning by gradually increasing command velocity range and magnitude of external forces and torque. In each episode, the external disturbances are applied four times at randomly sampled timesteps with random force impact duration T_F . Dynamics uncertainties and sensor noise are applied to reduce the sim to real gap. The domain randomization details are shown in Table III.

IV. SIMULATION EXPERIMENTS

In this section, we present the results of various simulation experiments, analysis of our method and comparison with baseline methods. Specifically, we answer the following questions: **Q1** Does our switched-policy method achieve both adjustable compliance locomotion and safety under a wide range of external force disturbances? **Q2** How does the tunable parameter ϵ affect the performance? **Q3** Is the teacher-student training framework necessary and effective? **Q4** How does our method compare to other baseline methods?

A. Metrics and Baselines

We consider the following metrics to evaluate performance:

1) Effective compliance range (s/kg): $\Delta C = C_{\text{high}} - C_{\text{low}}$, where C is the directional effective compliance based on the velocity response to external forces calculated as:

$$C = \frac{1}{|\mathcal{T}_{\mathcal{F}}|} \sum_{t \in \mathcal{T}_{\mathcal{F}}} \frac{(\mathbf{v}(t) - \mathbf{v}'(t))^\top \mathbf{F}_{xy}(t)}{\mathbf{F}_{xy}^\top(t) \mathbf{F}_{xy}(t)}, \quad \mathcal{T}_{\mathcal{F}} = \{t \mid \|\mathbf{F}_{xy}(t)\| > 0\}, \quad (13)$$

which quantifies the velocity response of the robot along the direction of the applied external force. C_{high} and C_{low} correspond to the effective compliance obtained using the highest and lowest compliance parameter settings of each controller. A larger ΔC indicates a wider achievable compliance range.

2) Command velocity tracking error (m/s): The episode-average command velocity tracking error during force-free timesteps computed as

$$e_v = \frac{1}{|\mathcal{T}|} \sum_{t \in \mathcal{T}} \|\mathbf{v}(t) - \mathbf{v}'(t)\|_2, \quad \mathcal{T} = \{t \mid \|\mathbf{F}_{xy}(t)\|_2 = 0\}, \quad (14)$$

A lower e_v indicates that the robot recovers faster from external disturbance to execute the command velocity.

3) Success rate (%): $SR = \frac{N_{\text{success}}}{N_{\text{disturbances}}} \times 100\%$, where N_{success} is the number of times in which the robot maintains locomotion without failure, and $N_{\text{disturbances}}$ is the total number of disturbance occurrence.

4) Average power (W): The episode-average power consumed by all motors, calculated as

$$P_{\text{motor}} = \frac{1}{t_f} \sum_i \int_0^{t_f} |\tau_i(t) \dot{q}_i(t)| dt. \quad (15)$$

We compare our approach against two representative learning-based force compliant locomotion baseline controllers:

TABLE III
DOMAIN RANDOMIZATION PARAMETER

	Term	Value
Dynamics	Robot mass	$\mathcal{U}(12.75, 17.25)$ kg
	Friction coefficient	$\mathcal{U}(0.1, 2.0)$
	Joint K_p gain	$\mathcal{U}(19, 21)$
	Joint K_d gain	$\mathcal{U}(0.48, 0.52)$
	ERFI-50 [20]	$0.78\text{Nm} \times \text{Curriculum}$
	Joint bias	$\mathcal{U}(-0.08, 0.08)$
Sensor noises	Base angular velocity	$\mathcal{U}(-0.25, 0.25)$ rad/s
	Gravity vector	$\mathcal{U}(-0.1, 0.1)$
	Joint positions	$\mathcal{U}(-0.015, 0.015)$ rad
	Joint velocities	$\mathcal{U}(-1.5, 1.5)$ rad/s
Disturbances	$F_{x,y}$	$\mathcal{U}(-700, 700)$ N
	F_z	$\mathcal{U}(-50, 50)$ N
	$\tau_{x,y}$	$\mathcal{U}(-50, 50)$ Nm
	τ_z	$\mathcal{U}(-20, 20)$ Nm
	T_F (Impact duration)	$\mathcal{U}(0.5, 3)$ sec
Commands	k	$\mathcal{U}(0.0, 0.1)$
	v_x^f	$\mathcal{U}(-2.5, 2.5)$ m/s
	v_y^f	$\mathcal{U}(-2, 2)$ m/s
	ω_z	$\mathcal{U}(-1.5, 1.5)$ rad/s

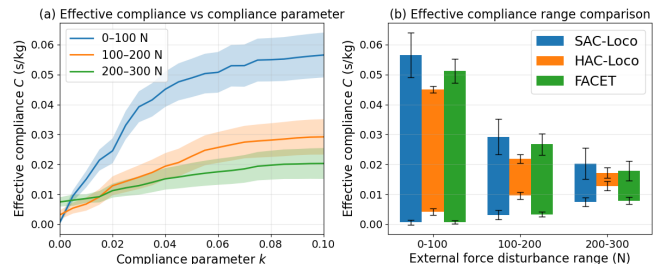


Fig. 3. (a): Average effective compliance over the compliance parameters for different range of disturbance magnitude. (b): Effective compliance range of different methods.

1) HAC-LoCo [12]: A hierarchical reinforcement learning framework designed for quadruped locomotion under continuous external disturbances. We use $\beta = 10$ and $\beta = 1000$ as the highest and lowest compliance setting.

2) FACET [13]: A reinforcement learning-based impedance tracking controller that enforces compliance by tracking the dynamics of a virtual mass-spring-damper model. We use $K_p = 0, K_d = 4$ and $K_p = 48, K_d = 13.85$ as the highest and lowest compliance setting.

We re-implemented both baselines using the same disturbance settings as our method.

B. Evaluation on compliance and safety

We use safety threshold $\epsilon = 0.9$ for the following simulation experiments. We first evaluate the compliance performance of SAC-LoCo by applying external force disturbances in three different magnitude ranges: $|\mathbf{F}| \in [0 \sim 100]\text{N}$, $|\mathbf{F}| \in [100 \sim 200]\text{N}$ and $|\mathbf{F}| \in [200 \sim 300]\text{N}$. For each compliance parameter k , we conduct 40,000 evaluation episodes with randomized commands in Table III. We compute the directional effective compliance C using (13) for each disturbance. As shown in Fig. 3 (a), the average effective compliance C increases monotonically with the compliance parameter k , demonstrating that SAC-LoCo enables adjustable compliance. For larger force ranges, the

TABLE IV
PERFORMANCE UNDER DIFFERENT RANGE OF EXTERNAL FORCE IN SIMULATION. (MEAN \pm STD DEV)

	SR (%)	\bar{e}_v (m/s)	\bar{P}_{motor} (W)	SR (%)	\bar{e}_v (m/s)	\bar{P}_{motor} (W)	SR (%)	\bar{e}_v (m/s)	\bar{P}_{motor} (W)
	$ F = 0 \sim 100N$			$ F = 100 \sim 200N$			$ F = 200 \sim 300N$		
SAC-LoCo (ours)	100	0.111 \pm 0.022	151.9 \pm 17.8	99.84	0.127 \pm 0.024	160.8 \pm 21.7	99.30	0.146 \pm 0.024	175.8 \pm 23.2
HAC-LoCo [12]	99.74	0.115 \pm 0.027	178.2 \pm 22.3	94.15	0.121 \pm 0.029	196.4 \pm 29.3	67.31	0.148 \pm 0.030	217.1 \pm 27.2
FACET [13]	99.96	0.158 \pm 0.041	165.8 \pm 19.2	93.65	0.172 \pm 0.055	172.3 \pm 23.8	80.84	0.195 \pm 0.062	189.2 \pm 24.6
	$ F = 300 \sim 400N$			$ F = 400 \sim 500N$			$ F = 500 \sim 600N$		
SAC-LoCo (ours)	96.62	0.183 \pm 0.041	192.8 \pm 26.9	91.59	0.232 \pm 0.061	232.5 \pm 30.8	84.11	0.294 \pm 0.083	255.7 \pm 31.5
HAC-LoCo [12]	43.62	0.196 \pm 0.038	220.4 \pm 19.3	28.63	0.275 \pm 0.052	225.2 \pm 20.6	18.22	0.357 \pm 0.065	231.2 \pm 18.3
FACET [13]	72.23	0.231 \pm 0.073	215.2 \pm 23.1	56.35	0.306 \pm 0.071	223.7 \pm 28.2	35.93	0.368 \pm 0.080	228.5 \pm 28.8

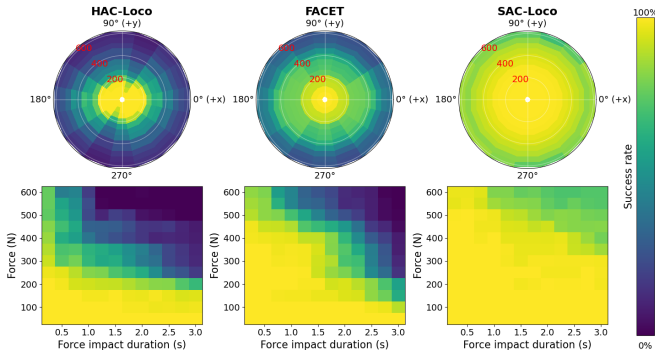


Fig. 4. Top: Polar heatmap showing the success rate under different force magnitude and direction of force relative to robot’s heading. Bottom: Heatmap showing success rate under different force magnitude and impact duration.

increase in C becomes less pronounced due to the maximum velocity limits of the robot. Fig. 3 (b) compares the achievable compliance range ΔC with baseline methods. SAC-LoCo achieves a larger ΔC than HAC-LoCo and FACET, indicating a wider range of achievable compliance behaviors.

To evaluate the safety against external disturbances, we systematically test our method under different external force magnitudes $|F| \in [50, 100, 150, \dots, 600]N$, impact directions relative to robot’s heading $\theta_F \in [0, \pi/8, \pi/4, \dots, 2\pi]$ rad, and impact durations $T_F \in [0.25, 0.5, \dots, 3.0]$ s, resulting in a total of 2304 disturbance configurations. Each configuration is evaluated with 30 episodes with randomized commands in Table III. The compliance level for all methods are set to the maximum values. We calculated the SR for all disturbance configurations. Fig. 4 (top) illustrates the SR averaged over all T_F for each (F_{xy}, θ_F) . HAC-LoCo’s SR exhibits a noticeable decrease in SR when F is applied along the lateral direction (y -axis) of the robot. FACET achieves overall higher SR than HAC-LoCo, but also has slight decrease in SR under lateral disturbances. SAC-LoCo outperforms both baselines and maintains a more uniform SR across all θ_F , demonstrating improved robustness to external forces. Fig. 4 (bottom) illustrates the SR averaged over all θ_F for each (F_{xy}, T_F) . HAC-LoCo achieves good SR with low $|F|$ but more failures with larger $|F|$. FACET achieves better SR for larger $|F|$ but still fails under longer T_F . SAC-LoCo maintains higher SR under both larger $|F|$ and longer T_F than baselines. Table IV summarizes the performance. It is shown that SAC-LoCo consistently achieves higher SR than baselines. SAC-LoCo consumes less

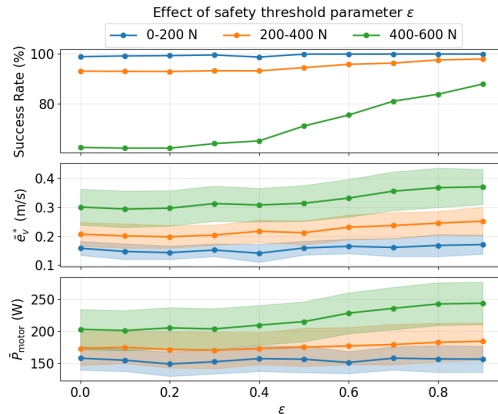


Fig. 5. The effect of the safety critic output threshold ϵ on SAC-LoCo’s performance under different force disturbance ranges.

power than baselines except when F exceeds 400N. SAC-LoCo also achieves lower e_v , suggesting it restores the robot from disturbance compliance to velocity tracking faster. The results show that SAC-LoCo achieves better safety without sacrificing on command tracking.

C. Effect of different ϵ for policy switching

ϵ determines the threshold for policy-switching. To investigate the sensitivity of ϵ and how switching to π_{safe} affect performance, we perform simulation experiments across different values of $\epsilon \in [0, 0.1, 0.2, \dots, 0.9]$. For each ϵ , we conduct 40,000 evaluation episodes and calculate the SR and \bar{P}_{motor} . In addition, we calculate the velocity tracking error between robot’s velocity and the desired velocity v^* generated from the velocity modulator as $e_v^* = \frac{1}{T} \sum_{t=0}^T \|v(t) - v^*(t)\|_2$, a larger e_v^* indicates more deviation from the compliance behavior of π_{comply} . Fig. 5 shows that when $|F| < 200N$, the performance is insensitive to changes in ϵ , indicating that π_{safe} is rarely activated under moderate disturbance. This suggests that the output of V_{safe} accurately characterizes the safety condition of the robot. For $|F| > 200N$, setting $\epsilon = 0$ (using only π_{comply}) leads to a decrease in SR . As ϵ increases, SR improves, indicating that switching to π_{safe} helps the robot recover to safe states. Meanwhile, increasing ϵ results in only marginal increase in e_v^* and P_{motor} , indicating that our method improves safety without significantly compromising compliance and energy usage.

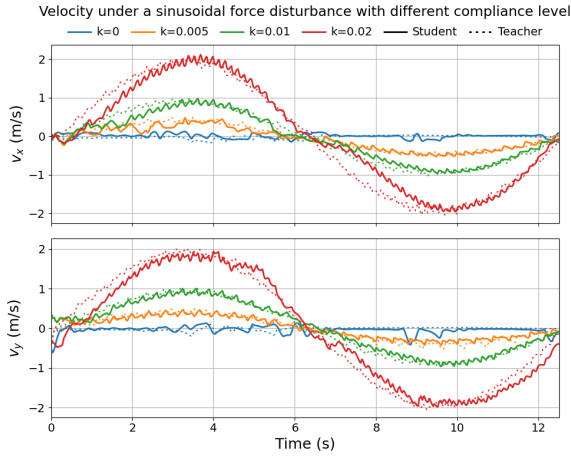


Fig. 6. Velocity of the robot under a sinusoidal force disturbance: $F_x = F_y = 100\sin(0.5t)$ with different compliance parameters. Dashed line is teacher and solid line is student.

TABLE V
ABLATION ON SAC-LOCO

	SR (%)	$\bar{\epsilon}_v^*$ (m/s)	\bar{P}_{motor} (W)
$ F = 0 \sim 300N$			
SAC-LoCo (Teacher)	99.78	0.171 ± 0.011	158.7 ± 14.2
SAC-LoCo (Ours)	99.71	0.190 ± 0.035	162.8 ± 23.2
SAC-LoCo w/o teacher	70.21	0.719 ± 0.253	221.2 ± 25.8
π_{safe} w/o o'_{unsafe}	99.36	0.198 ± 0.041	168.8 ± 15.2
π_{safe} w/o CCP	92.13	0.194 ± 0.033	183.8 ± 22.4
SAC-LoCo w/o V_{safe}	99.42	0.207 ± 0.090	195.8 ± 39.2
$ F = 300 \sim 600N$			
SAC-LoCo (Teacher)	93.81	0.252 ± 0.023	219.6 ± 20.1
SAC-LoCo (Ours)	90.77	0.285 ± 0.092	227.0 ± 39.5
SAC-LoCo w/o teacher	21.19	1.283 ± 0.552	275.8 ± 31.4
π_{safe} w/o o'_{unsafe}	85.21	0.288 ± 0.085	211.4 ± 30.6
π_{safe} w/o CCP	30.96	0.454 ± 0.140	262.9 ± 36.0
SAC-LoCo w/o V_{safe}	68.38	0.659 ± 0.189	237.1 ± 37.7

D. Policy distillation performance

To verify that our teacher-student framework helps the robot to learn external disturbance with only proprioceptive sensing, we compare the performance of teacher policies with performance of student policies to verify the effectiveness of policy distillation. Fig. 6 shows that π_{comply} successfully achieves different compliance levels under a sinusoidal force, tracking v^* with small tracking errors as compared to π_{comply}^* . We further conduct 40,000 episodes and calculated performance metrics using the teacher’s policies. Table V shows that the student policy performs slightly below the teacher policy. This result validates that the distillation framework successfully preserves compliance and recovery capabilities while removing reliance on privileged force information, making the policy suitable for real-world deployment.

E. Ablation studies on SAC-LoCo

We perform the following ablation studies:

1) **SAC-LoCo w/o teacher**: We train π_{comply} and π_{safe} directly using student observations as (5) with the same training setup.

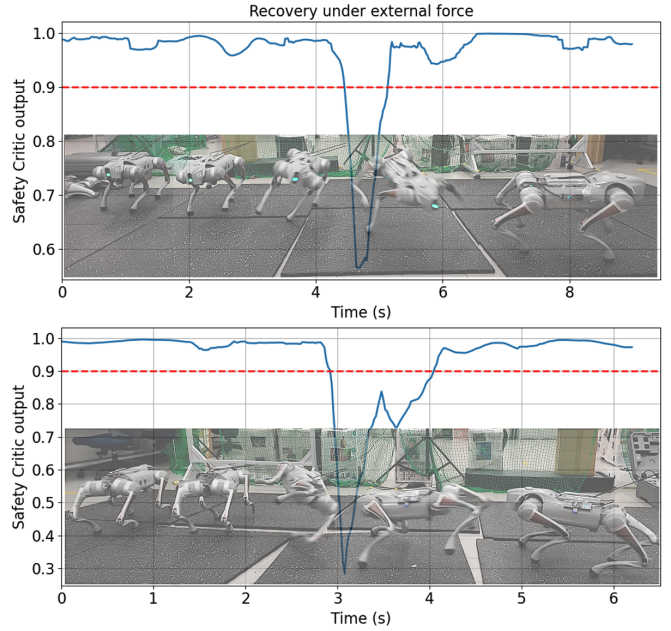


Fig. 7. Two example cases when the robot being dragged and losing balance. V_{safe} outputs a value below $\epsilon = 0.9$ and π_{safe} takes over to restore balance. After output of V_{safe} increases above 0.9, π_{comply} is switched back. In both cases, robot restores balance and adjust the heading to align its x -axis with the force direction.

2) **π_{safe} w/o o'_{unsafe}** : We train π_{safe} without using o'_{unsafe} as state initializations.

3) **π_{safe} w/o CCP**: We train π_{safe} without the two stage training and without using the corrected capture point as recovery heuristic. We directly use reward to penalize collision and failure.

4) **SAC-LoCo w/o V_{safe}** : We replace V_{safe} with a rule-based policy switching state machine such that the system switches to π_{safe} when $\|\omega_{xy}\|_2 > 1$ rad/s.

As shown in Table V. The teacher-student training framework is necessary. Without the teacher’s guidance, π_{comply} cannot track v^* and π_{safe} is unable to recover the robot due to unobservable F and v^* , resulting in more failure, worse velocity tracking and more power usage. Removing o'_{unsafe} as state initialization slightly decreases SR . Training π_{safe} without CCP dynamics drastically decrease SR , indicating the effectiveness of using CCP to recover robot from unsafe states. Using rule based policy switching also results in more failure, highlighting the effectiveness of the safety critic.

V. HARDWARE DEPLOYMENT

We deploy SAC-LoCo onto the Unitree Go2 quadruped robot. The policy runs at 50 Hz on the Unitree Go2 Jetson Orin NX. We perform experiments to verify our policy’s effectiveness.

First, we test the compliance by using another quadruped robot to pull the robot with our policy. Given different compliance parameter, the robot can either resist the pulling force or comply with the force. We also tied the robot to an office chair with a person in the seat. The robot is given a constant velocity command of $v'_x = 0.6m/s$. The total weight of chair and person is around 70 kg. As shown in



Fig. 8. Quadruped robot is connected to an office chair with a seated person, and the robot is set to a constant velocity command of $v'_x = 0.6$ m/s to pull the chair forward. By adjusting different values of k , the pulling speed is varied.

Fig. 8, the robot's pulls the chair with lower speed as k increases.

Second, we evaluate safety under large external disturbances by dragging the robot using a rope connected to a digital force gauge. The robot is pulled by a person with the intent of inducing a failure, while the digital force gauge records the peak force F_{peak} applied during each pull. We collect 5 failures for each baseline. Among the 5 failures, HAC-LoCo experiences an average $F_{\text{peak}} = 120.4$ N. FACET experiences an average $F_{\text{peak}} = 193.8$ N. In contrast, SAC-LoCo has 0 failures in this experiment. Fig. 7 shows two example cases where the robot switches from π_{comply} to π_{safe} promptly to restore balance during an external force disturbance. Fig. 7 (top) shows when force is toward the head of the robot, the robot turns to align its head with the force. In contrast, Fig. 7 (bottom) shows that when the force is toward the tail of the robot, the robot turns to align its tail with the force.

Third, we set the maximum velocity command $v'_x = 2.5$ m/s with compliance parameter $k = 0$. We pull the robot using rope with the digital force gauge in the opposite direction and measure the largest pulling force that the robot can exert while maintaining stable locomotion without failure. The largest forward and backward pulling forces are 10.54 kg and 10.45 kg, respectively. This outperforms the 7.5 kg and 10 kg forward and backward pulling force reported in FACET [13].

VI. CONCLUSION

This paper presented SAC-LoCo, a novel safety-aware force compliant controller for quadruped robots to achieve adjustable compliant velocity tracking under external disturbances and robustness against large impulses. Extensive simulation and hardware experiments validate the effectiveness and practicality of SAC-LoCo. Compared with previous work, our approach broadens the compliance and safety of a quadruped under wider range of external forces. This work opens avenues for future research including adaptive adjustment of compliance level in response to varying environments and integration of the safety mechanism into highly dynamic quadruped maneuvers.

REFERENCES

[1] X. Cheng, K. Shi, A. Agarwal, and D. Pathak, "Extreme parkour with legged robots," in *Proceedings of the 2024 IEEE International*

Conference on Robotics and Automation (ICRA). Yokohama, Japan: IEEE, 2024, pp. 11 443–11 450.

[2] Y. Ji, G. B. Margolis, and P. Agrawal, "Dribblebot: Dynamic legged manipulation in the wild," in *Proceedings of the 2023 IEEE International Conference on Robotics and Automation (ICRA)*. IEEE, 2023.

[3] P. Arm, M. Mittal, H. Kolvenbach, and M. Hutter, "Pedipulate: Enabling manipulation skills using a quadruped robot's leg," in *Proceedings of the 2024 IEEE International Conference on Robotics and Automation (ICRA)*, Yokohama, Japan, 2024, pp. 5717–5723.

[4] T. He, B. Lan, R. Hasani, and D. Rus, "Agile but safe: Learning collision-free high-speed legged locomotion," *arXiv preprint arXiv:2401.17583*, 2024.

[5] H. Kim, H. Oh, J. Park, Y. Kim, D. Youm, M. Jung, M. Lee, and J. Hwangbo, "High-speed control and navigation for quadrupedal robots on complex and discrete terrain," 2025.

[6] C. Zhang, J. Jin, J. Frey, N. Rudin, M. Mattamala, C. Cadena, and M. Hutter, "Resilient legged local navigation: Learning to traverse with compromised perception end-to-end," in *2024 IEEE International Conference on Robotics and Automation (ICRA)*, Yokohama, Japan, 2024, pp. 34–41.

[7] J. Kang, H.-B. Kim, B.-I. Ham, and K.-S. Kim, "External force adaptive control in legged robots through footstep optimization and disturbance feedback," *IEEE Access*, vol. 12, pp. 157 531–157 539, 2024.

[8] Z. Xiao, J. Huang, Q. Gong, D. Fan, Z. Liu, and F. Gao, "Pa-loco: Learning perturbation-adaptive locomotion for quadruped robots," in *2024 IEEE/RSJ International Conference on Intelligent Robots and Systems (IROS)*. IEEE, 2024.

[9] N. Khandelwal, A. Manu, S. S. Gupta, M. Kothari, P. Krishnamurthy, and F. Khorrami, "Compliant control of quadruped robots for assistive load carrying," 2025.

[10] A. Hartmann, D. Kang, F. Zargarbashi, M. Zamora, and S. Coros, "Deep compliant control for legged robots," in *Proceedings of the 2024 IEEE International Conference on Robotics and Automation (ICRA)*, Yokohama, Japan, 2024, pp. 11 421–11 427.

[11] P. Li, H. Li, G. Sun, J. Cheng, X. Yang, G. Bellegarda, M. Shafiee, Y. Cao, A. Ijspeert, and G. Sartoretti, "Sata: Safe and adaptive torque-based locomotion policies inspired by animal learning," 2025.

[12] X. Zhou, X. Zhang, T. Wu, Q. Zhang, and L. Zhang, "Hac-loco: Learning hierarchical active compliance control for quadruped locomotion under continuous external disturbances," in *2025 IEEE/RSJ International Conference on Intelligent Robots and Systems (IROS)*, Hangzhou, China, 2025, pp. 10 649–10 655.

[13] B. Xu, H. Weng, Q. Lu, Y. Gao, and H. Xu, "Facet: Force-adaptive control via impedance reference tracking for legged robots," 2025.

[14] Q. Zhang, G. Han, J. Sun, W. Zhao, C. Sun, J. Cao, J. Wang, Y. Guo, and R. Xu, "Distillation-ppo: A novel two-stage reinforcement learning framework for humanoid robot perceptive locomotion," 2025.

[15] T. Xu, Y. Cheng, P. Shen, and L. Zhao, "Acl: Action learner for fault-tolerant quadruped locomotion control," 2025.

[16] J. Pratt, J. Carff, S. Drakunov, and A. Goswami, "Capture point: A step toward humanoid push recovery," in *2006 6th IEEE-RAS International Conference on Humanoid Robots*, Genova, Italy, 2006, pp. 200–207.

[17] D. Jain, A. Iscen, and K. Caluwaerts, "Hierarchical reinforcement learning for quadruped locomotion," 2019.

[18] V. Makoviychuk, L. Wawrzyniak, Y. Guo, M. Lu, K. Storey, M. Macklin, D. Hoeller, N. Rudin, A. Allshire, A. Handa, and G. State, "Isaac gym: High performance gpu-based physics simulation for robot learning," 2021.

- [19] J. Schulman, F. Wolski, P. Dhariwal, A. Radford, and O. Klimov, "Proximal policy optimization algorithms," 2017.
- [20] L. Campanaro, S. Gangapurwala, W. Merkt, and I. Havoutis, "Learning and deploying robust locomotion policies with minimal dynamics randomization," 2023.